ACS APPLIED MATERIALS & INTERFACES

Research Article

www.acsami.org

P3HT-Based Nanoarchitectural Fano Solar Cells

Wen-Pin Liao,[†,∥] Yen-Hsun Su,[‡,∥] Yun-Kai Huang,[§,∥] Chen-Sheng Yeh,[§] Li-Wen Huang,[‡] and Jih-Jen Wu*[,†]

[†]Department of Chemical Engineering, National Cheng Kung University, Tainan 701, Taiwan

[‡]Department of Materials Science and Engineering, National Cheng Kung University, Tainan 701, Taiwan

[§]Department of Chemistry, National Cheng Kung University, Tainan 701, Taiwan

Supporting Information

ABSTRACT: The finite difference time domain simulation shows the existence of an asymmetric quadrupole of Fano resonance on the surface of a gold−silica core−shell (Au@silica) nanoparticle (NP) as being incorporated into the metal oxide nanoarchitecture/P3HT hybrid. Compared to the metal oxide nanoarchitecture/P3HT hybrid solar cell, a 30% enrichment of the short-circuit current density (J_{sc}) is attained in the P3HT-based nanoarchitectural Fano solar cell with the Au@silica NPs. The enhancement of charge separation in the cell by the electric field of the Fano resonance is directly evidenced by time-resolved photoluminescence measurements. The increase of the degree of P3HT order in the hybrid by the incorporation of Au@silica NPs into the hybrid active layer may also contribute to the enhancement in the J_{sc}. Charge carrier dynamic measurements show that an electron collection efficiency of ∼97% can be maintained in the P3HT-based nanoarchitectural Fano solar cell. Significant improvement of the efficiency of the inverted metal oxide/P3HT hybrid solar cell is therefore achieved.

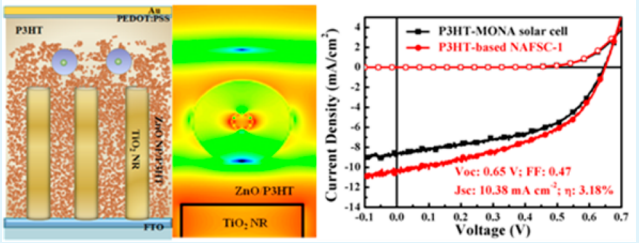

KEYWORDS: *hybrid polymer solar cell, metal oxide nanoarchitecture, gold−silica sore-shell nanoparticle, Fano resonance, charge dynamics*

1. INTRODUCTION

Polymer solar cells have attracted extensive attention for the potential application to renewable power sources for portable electronic devices because they can be fabricated at low cost, are lightweight, and have good mechanical flexibility.[1−3] The most representative configuration of polymer-based photovoltaic devices is the bulk heterojunction (BHJ) structure,[4,5] which is composed of electron acceptors blended into the electron donating conjugated polymer matrix. In addition to C_{60} derivatives, inorganic oxide nanocrystals have been employed to be electron acceptors for improving the stability of polymer solar cells.[1] Due to the low carrier mobilities of polymer materials and insufficient connectivity of electron acceptors, the thickness of the active layer of BHJ polymer-based solar cells is optimized to be 100−200 nm as a trade-off between light absorption and charge transport.[6]

For improving the light absorption in the thickness-limited BHJ active layer, the incorporation of noble metal nanoparticles (NPs), which exhibit localized surface plasmonic resonance (LSPR) at specific wavelengths, into the polymer solar cells have been reported to be a promising light trapping method.[6,7] With the strong resonant charge density oscillations on the surfaces of the metal NPs via LSPR excitation, NPs behave as light scattering centers to improve light trapping in the active layer. Moreover, NPs may serve as subwavelength antennas in the active layer to increase the effective absorption cross-section and exciton dissociation by the enhanced local electromagnetic fields.[6,8−10] Due to the high surface recombination velocity of the bare metallic NPs, core−shell NPs composed of the plasmonic metal NPs shielded by an ultrathin insulator (metal@ultrathin insulator NPs) have been incorporated into the active layers to prevent the recombination of photocarriers on the surfaces of plasmonic NPs.[11−13] We have reported a nanoarchitectural hybrid polymer solar cell with an active layer integrating bulk and ordered heterojunction oxide/polymer hybrids, that is, in situ-generated ZnO/poly(3-hexylthiophene) scaffolded by a TiO_2 nanorod (NR) array.[14] A high electron collection efficiency is demonstrated in the TiO_2 NR−ZnO NP/P3HT hybrid polymer solar cell, which is ascribed to the TiO_2 NR array in the hybrid serving as an efficient electron transporter/collector extended from fluorine-doped tin oxide (FTO) electrode. Moreover, the TiO_2 NR array also functions as a scaffold to hold the sufficient amount of ZnO NP/P3HT hybrid. With these characteristics of TiO_2 NR array, the thickness of the active hybrid layer can therefore be thickened for increasing the light harvesting efficiency.

It has been reported that adding dielectric to plasmonic structures will produce Fano resonances by the interactions between dielectric and plasmon resonant modes.[15,16] A P3HT-based nanoarchitectural Fano solar cell (NAFSC) is demon-

Received: July 23, 2014
Accepted: September 16, 2014
Published: September 16, 2014

strated in this work. Instead of plasmonic metal NPs or metal@ultrathin insulator NPs, the gold−silica core−shell (Au@silica) NPs, where the diameter of the Au core is ∼10 nm and the thickness of the silica shell is ∼20 nm, are incorporated to the TiO_2 NR−ZnO NP/P3HT hybrid active layer. The finite difference time domain (FDTD) simulation shows the existence of an asymmetric quadrupole of Fano resonance on the surface of Au@silica NP within the P3HT/metal oxide nanoarchitecture (P3HT−MONA) hybrid. A 30% enrichment of the short-circuit current density (J_{sc}) of the P3HT−MONA hybrid solar cell is attained by the incorporation of Au@silica NPs in the active layer. The increase of the degree of P3HT order in the hybrid by the incorporation of the Au@silica NPs is determined by Raman characterization. Charge carrier dynamics in the P3HT-based NAFSC are investigated under the illumination of Fano resonance-matched green light. Time-resolved photoluminescence (TRPL) measurements directly evidence that with the addition of the Au@silica NPs, charge separation in the P3HT−MONA hybrid is enhanced by the Fano resonance-induced electric field. Moreover, an electron collection efficiency of ∼97%, which is determined by impedance spectroscopy (IS) and intensity-modulated photocurrent spectroscopy (IMPS), can be maintained in the P3HT-based NAFSC.

2. EXPERIMENTAL METHODS

2.1. Device Fabrication. Aligned rutile TiO_2 NR arrays were grown on FTO substrates by a hydrothermal method.[14,17−19] The thickness of the TiO_2 NR array was determined by the growth period. Au NPs with an average size of 10 nm were synthesized via the following procedure. An aqueous solution of 1 mM $HAuCl_4$ was refluxed at 100 °C with constant stirring for 5 min. Then, 5 mL of 38.8 mM trisodium citrate was added into the solution, and the reflux was conducted for another 10 min. The silica shell was formed on the Au NPs following the reported method[20] with minor modifications. First, a solution containing 30 mL of ethanol, 7 mL of H_2O, and 380 μL of Au NPs (190 ppm) was stirred for 5 min. After 200 μL of (3-aminopropyl) trimethoxysilane (APMS) (10% in ethanol) was added to the stirred solution, the reaction was kept for 15 min followed by the addition of 4 μL of tetraethylorthosilicate (TEOS) and 180 μL of 0.1 M aqueous NaOH solution in sequence. The solution was then stirred for another 24 h. The resulting solution was centrifuged, and the Au@silica NPs were washed with ethanol. Finally, the Au@silica NPs were redispersed in tetrahydrofuran (THF). The active layer solutions containing diethylzinc (DEZ) (45 mg mL^{-1})/P3HT (45 mg mL^{-1}) in THF with various contents of Au@silica NPs were prepared inside a glovebox. The P3HT used had a molecular weight of M_w = 80000 g mol^{-1}. To fabricate the solar cells, the active layer solution was infiltrated into the TiO_2 NR array on the FTO substrate by spin coating under a controlled relative humidity of 40% in N_2. A pristine P3HT film (300 nm) was then spin-coated (45 mg mL^{-1} in chlorobenzene) onto the hybrid film and was annealed at 150 °C for 10 min. A thin layer of PEDOT:PSS (Baytron PVP AL 4083) was further spun onto the pristine P3HT overlayer in air followed by heat treatments at 120 and 150 °C for 6 and 3 min, respectively. Finally, a 100 nm thick gold layer was deposited on top of the PEDOT:PSS layer.

2.2. Characterization of Hybrid Solar Cells. Optical absorptions of the hybrids were measured using a UV−vis−IR spectrophotometer (JASCO V-670). The degree of P3HT order in the hybrids was characterized by Raman spectroscopy (integrated by Protrustech Corporation Limited) at an excitation length of 532 nm. Photovoltaic characteristics of the solar cells were measured under AM-1.5 simulated sunlight at 100 mW cm^{-2} (300 W, model 91160A, Oriel). A black-painted mask on the FTO substrate side was used to create an exposed area of 0.04 cm^2 for all solar cells with island-type electrodes.[21] External quantum efficiency (EQE) was measured using a 500 W xenon light source (Oriel) and a monochromator (Oriel Cornerstone) equipped with a Si detector (model 71640, Oriel). The power of an additional green-laser-light bias was 4 mW. Measurements of TRPL spectroscopy were performed using a pulse laser (405 nm) with a pulse width of 70 ps for excitation. The TRPL decays at 710 nm were recorded by a time-correlated single-photon counting (TCSPC) spectrometer. Measurements of IS were carried out under the illumination of a green LED light (530 nm) with various intensities by applying a 10 mV AC signal over the frequency range of $1−10^5$ Hz at V_{OC} of the hybrid solar cells using a potentiostat with a frequency response analyzer (FRA, Zahner, IM6ex). A two-channel transmission line model was employed to investigate the electron transport and recombination in the hybrid solar cells.[22] Measurements of IMPS were conducted under a modulated green LED light (530 nm) driven by a source supply (Zahner, PP210) and a potentiostat with a FRA (Zahner, IM6ex). The light intensity modulation was 20% of the base light intensity over the frequency range of $1−10^4$ Hz. The illumination intensity is variable in the range of 30−90 mW cm^{-2}. The method for extraction of electron transit times in the hybrid solar cells from the IMPS responses has been described in detail elsewhere.[23] FDTD method[11,24] (R-soft Fullwave) has been employed to simulate electromagnetic energy density of the Fano-P3HT−MONA hybrid with a 530 nm continuous EM wave entering from the TiO_2 NR array side and the ten-layered perfectly matched layers as the boundary condition. The spacial grid number is 2940000, and the time step is 0.00057 μm.

3. RESULTS AND DISCUSSION

Figure 1a shows the schematic of the P3HT-based NAFSC. Au@silica NPs are incorporated to the TiO_2 NR-array-

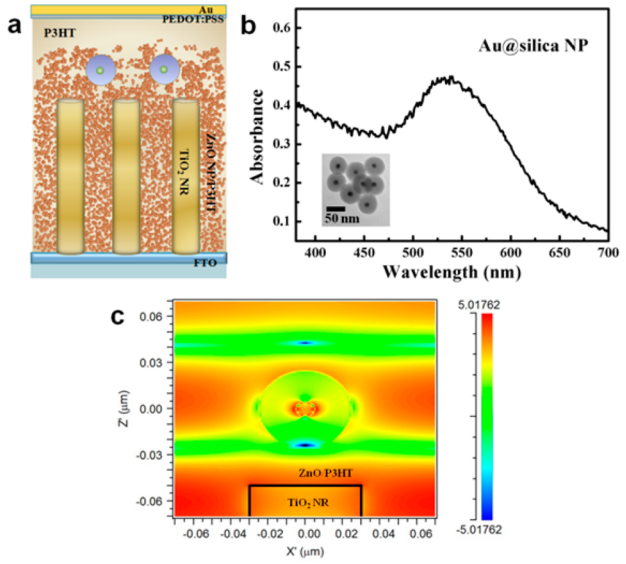

Figure 1. (a) Schematic of P3HT-based NAFSC. (b) Absorption spectrum of Au@silica NPs dispersed in ethanol and (inset) TEM image of Au@silica NPs. (c) Simulated energy density distribution around Au@silica NP in ZnO NP/P3HT hybrid with a 530 nm continuous EM wave entering from the TiO_2 NR array side.

scaffolded ZnO NP/P3HT hybrid active layer[14] by infiltrating a diethylzinc/Au@silica NP/P3HT solution into the interstices of the ordered TiO_2 NR array under a relative humidity of 40% in ambient N_2. A layer of ZnO NP/Au@silica NP/P3HT hybrid (referred to as "overlayer" hereafter) is developed on the top of the TiO_2 NR array from the precursor solution remaining on the NR array after spinning. A pristine P3HT layer is additionally spin-coated on the top of the active layer. The TEM image of the Au@silica NPs is shown in the inset of

Figure 1b. The average size of the Au@silica NPs is 50 nm, where the diameter of the Au core is ~10 nm and the thickness of the silica shell is ~20 nm. The absorption spectrum of the Au@silica NP solution in ethanol is displayed in Figure 1b. It reveals that the absorption of Au@silica NPs is in the wavelength range of 450−650 nm with a maximum absorption peak at 535 nm. In this work, the Au@silica NPs content incorporated into the P3HT−MONA hybrid is represented by the concentration of gold (ppm) in the precursor solution of diethylzinc/Au@silica NP/P3HT. For simplicity, the Au@silica NP/P3HT−MONA hybrid prepared using the precursor solution with x ppm of Au is referred to as "Fano-P3HT−MONA-x" hereafter.

Figure 1c shows the FDTD simulation result of the electromagnetic (EM) energy density distribution in the Au@silica NP incorporated P3HT−MONA (TiO_2 NR−ZnO NP/P3HT) hybrid as a 530 nm continuous EM wave enters from the TiO_2 NR array side. Due to the absorption of 530 nm continuous wave by P3HT, the energy density is getting weak in the ZnO NP/P3HT domain when the continuous wave passes through the hybrid. As shown in Figure 1c, a quasi-static asymmetric quadrupole with dimensions of 20−30 nm appears on the surface of the silica shell. The electric fields of the asymmetric quadrupole are locally lower than those in the ZnO NP/P3HT domain far from the Au@silica NP. We suggest that the formation of the asymmetric quadrupole is mainly pertaining to the following reasons. As shown in Figure S1 (Supporting Information), the strong EM field of surface plasmonic resonance of Au NP core (regions enclosed by the black dashed lines) induces an opposite dipole on the surface of the silica shell (regions enclosed by blue dashed lines). The LSPR-induced electric field on the surface of Au@Silica NP is therefore detracted by coupling with the opposite induced dipole. Moreover, the quadrupolar electric mode (regions enclosed by white dashed lines) is developed on the surface of the silica shell because of symmetry breaking by the TiO_2 NR and the continuous waves of the incident light. The quadrupolar electric mode coupling with the detracted LSPR on the surface of the silica shell leads to the asymmetric quadrupole on the surface of the Au@silica NP in the hybrid, as shown in Figure 1c. The quasi-static asymmetric quadrupole is considered to be Fano resonance, which is essentially produced by the interactions between dielectric and plasmon resonant modes.[15,16]

Figure 2a shows the absorption spectra of the Fano-P3HT−MONA hybrids with various Au@silica-NP concentrations. The thickness of the TiO_2 NR array is 650 nm. The absorbances of the active layers in the wavelength range of 400−600 nm are not enhanced by the incorporation of Au@silica NPs, as shown in Figure 2a, which is dissimilar to the results demonstrated in the plasmonic BHJ polymer solar cells.[6] Moreover, in comparison with the pristine P3HT, the spectrum for which is also illustrated in the figure, the P3HT−MONA and Fano-P3HT−MONA hybrids possess wider absorption ranges with the absorption edges shifted to longer wavelengths. In the case of the P3HT−MONA hybrid, the decrease in the optical band gap of P3HT is ascribed to the increase of the degree of P3HT order as in situ formation of ZnO NPs in the hybrid.[14] Figure 2a shows that the internal order within the P3HT domain of the hybrid is also influenced by the addition of Au@silica NPs, which has been confirmed by the Raman peak position of the symmetric C═C stretch mode shown in Figure 2b and Table S1 (Supporting Information). A shift in

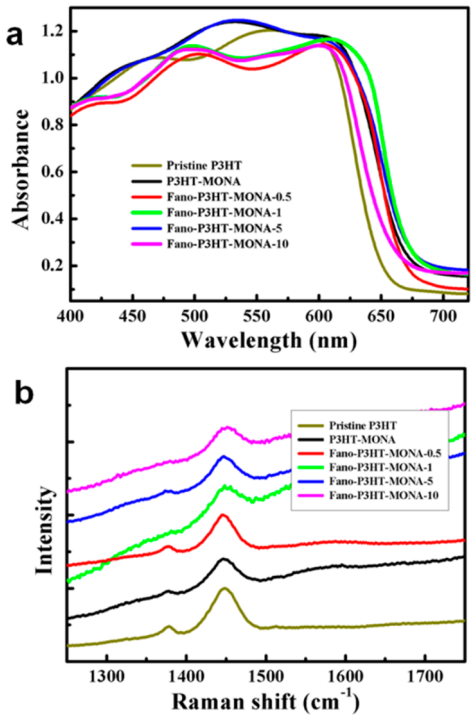

Figure 2. (a) UV−vis absorption spectra of pristine P3HT film and Fano-P3HT−MONA hybrids with various Au@silica-NP contents. (b) Raman spectra of pristine P3HT film and Fano-P3HT−MONA hybrids with various Au@silica NP contents.

the C═C mode peak position to a lower wavenumber indicates the higher degree of order in the hybrids.[25] The Raman characterizations reveal that with an appropriate Au@silica-NP content (i.e., 1−5 ppm), the crystallinity of the P3HT in the Fano-P3HT−MONA hybrid is improved further compared to those in the pristine P3HT film and MONA-P3HT hybrid.

The photocurrent density (J)−voltage (V) curves of the P3HT-based NAFSCs with various Au@silica NP contents (referred to as "P3HT-based NAFSC-x" hereafter) are shown in Figure 3a. For comparison, the J−V curve of the P3HT−MONA solar cell, which is also fabricated using the 650 nm thick TiO_2 NR array, is presented in this figure. The photovoltaic properties of these solar cells are summarized in Figure 3b. As the Au@silica NPs are incorporated into the active layer, the short-circuit current density (J_{sc}) of the hybrid polymer solar cell is significantly increased from 5.15 mA cm^{-2} to an optimized value of 6.79 mA cm^{-2}, monitored in P3HT-based NAFSC-1 solar cell. A 30% enrichment of the J_{sc} is attained in the P3HT-based NAFSC with an appropriate content of the Au@silica NPs. Conversely, the V_{OC} and FF of the P3HT-based NAFSC are slightly decreased as the Au@silica-NP content increases. Therefore, the efficiency of the P3HT-based NAFSC with an optimized concentration of Au@silica NPs is improved by 23.5%, from 1.74 to 2.15%. The statistical photovoltaic parameters of the P3HT−MONA and P3HT-based NAFSC-1 cells are shown in Figure S2 and Table S2 (Supporting Information).

The EQE spectra of the P3HT-based NAFSC-1 and the corresponding P3HT−MONA solar cell are shown in Figure 4a, revealing the enhancement of EQE values in the wavelength range of 350−700 nm as incorporating the Au@silica NPs into the active hybrid layer. The EQE modulation of the two cells is further illustrated in Figure 4b. A ~10% modulation of the EQE

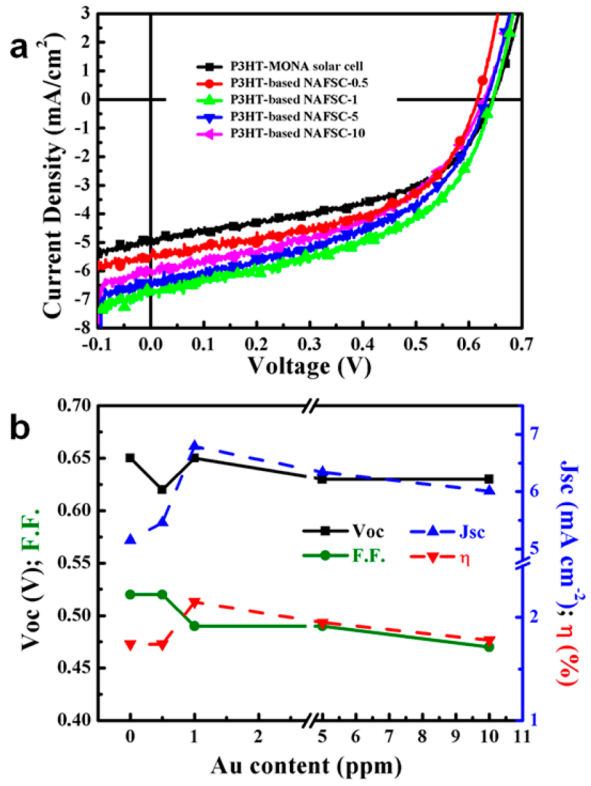

Figure 3. (a) *J*–*V* curves and (b) photovoltaic properties of P3HT-based NAFSCs with various Au@silica-NP contents. The thickness of TiO_2 NR array in cells is 650 nm.

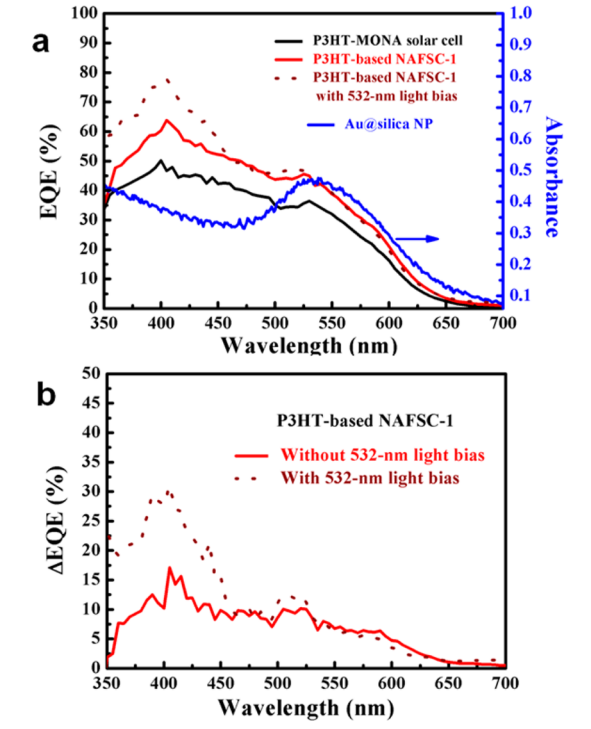

Figure 4. (a) EQE spectra of (black line) P3HT–MONA solar cell taken by ordinary way and P3HT-based NAFSC-1 (red solid line) without and (red dashed line) with an additional green light illumination, and (blue line) absorption spectrum of Au@silica NPs dispersed in ethanol.

values is obtained in the wavelength range of 375–525 nm, which does not comply with the absorption spectrum of Au@silica NPs shown in Figure 1b. The result shows that Fano resonance-induced EQE enrichment at specific wavelengths is not observed with the addition of Au@silica NPs.

It should be noted that the effect of Fano resonance on the solar cells is absent at the wavelengths out of the Au@silica NPs absorption range while conducting the ordinary EQE measurements. To further investigate the effect of Fano resonance on the EQE of the Au@silica-NP incorporated solar cell, we used an additional 532 nm light, which matches the absorption range of Au@silica NPs, to illuminate the P3HT-based NAFSC-1 during EQE measurements. The photocurrent contributed from the green light bias is eliminated for the calculation of the EQE values, and the corresponding EQE spectrum is shown in Figure 4a. It reveals that at the wavelengths out of the Au@silica NPs absorption range, the EQE values taken with the green light bias are significantly enhanced compared to those measured free of the green light bias, demonstrating that Fano resonance influences the EQE values of the Au@silica-NP incorporated cell. However, the EQE values of the P3HT-based NAFSC-1 with and without the green light bias are almost identical in the wavelength range of the Au@silica NP absorption. It is attributed to the effect of Fano resonance contributing to the EQE values of the P3HT-based NAFSC-1 in the wavelength range of the Au@silica NP absorption using the ordinary measurement method. With the green light bias, EQE modulation (compared to the EQE of the P3HT–MONA solar cell without the green light bias) is shown in Figure 4b. It reveals that the influence of Fano resonance also contributes to the enhancements of the EQE value at the wavelengths out of the Au@silica NP absorption range, suggesting that there are other influences of the Au@silica NP incorporation instead of Fano resonance-induced light absorption and trapping on the photovoltaic performance of the P3HT–MONA solar cells.

The steady-state PL measurements are conducted to examine the mechanism responsible for the photocurrent increase in the P3HT-based NAFSC-1. An excitation wavelength of 532 nm is employed, which matches with the resonance frequency of the Au@silica NP induced Fano resonances. It has been recognized that an increase in PL intensity of the plasmonic solar cell is ascribed to the enhancement of exciton generation rate due to the improved polymer light absorption induced by LSPR.[13,26,27] As shown in Figure 5a, the PL intensity of P3HT is quenched when Au@silica NPs are incorporated into a hybrid, indicating the steady-state exciton concentration is not increased in the P3HT-based NAFSC-1.

The dynamics of charge separation at interface between P3HT and the oxide nanostructures in the P3HT–MONA hybrids with and without the Au@silica NP addition are examined by TRPL using a 405 nm pulse laser for excitation. The TRPL decay curves of the P3HT–MONA and Fano-P3HT–MONA-1 hybrids at 710 nm are shown in Figure 5b. The average PL lifetimes of the P3HT–MONA and Fano-P3HT–MONA-1 hybrids are 215 and 211 ps, respectively. The 405 nm laser does not trigger the Fano resonance of the Au@silica NPs; therefore, the results show that the charge separation efficiencies in the two hybrids are similar in the absence of Fano resonance. Moreover, it reflects that the charge separation efficiency is not improved by creating a new interface of P3HT and silica through the incorporation of the Au@silica NPs into the hybrid. To investigate the coupling process between Fano resonance and the excitons, the TRPL

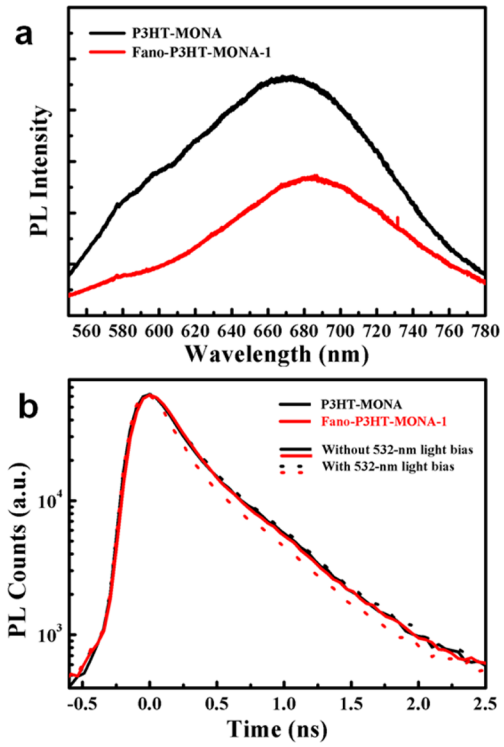

Figure 5. (a) Photoluminescence spectra of P3HT−MONA and Fano-P3HT−MONA-1 hybrids. (b) PL decay curves of P3HT−MONA and Fano-P3HT−MONA-1 hybrids (solid line) without and (dashed line) with green light illumination.

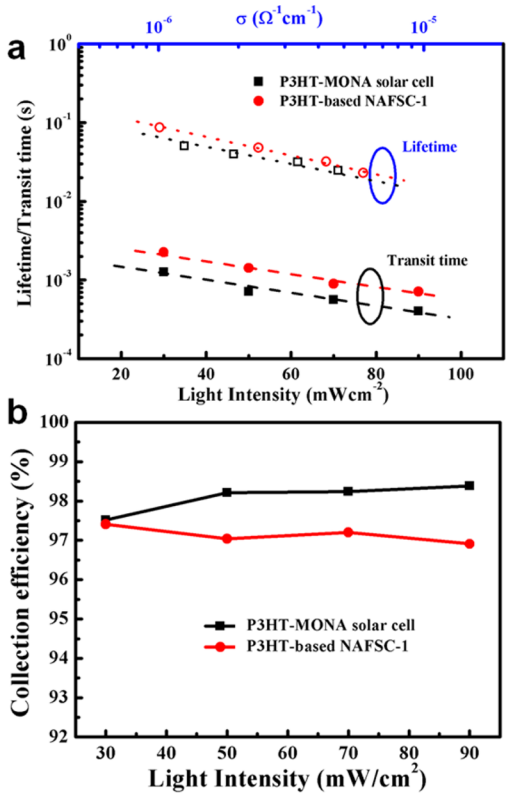

Figure 6. (a) Conductivity dependence of electron lifetimes and light intensity dependence of electron transit times in the P3HT−MONA solar cell and P3HT-based NAFSC-1. (b) Light intensity dependence of electron collection efficiencies in the two cells.

decay curves are further taken with an additional 532 nm light shining on the hybrids, which are also shown in Figure 5b. With the green-light irradiation, the PL lifetime of the P3HT−MONA hybrid remains at 215 ps, whereas the PL lifetime of the Fano-P3HT−MONA-1 hybrid is significantly reduced to 147 ps. The Au-content dependence of PL lifetime in the Fano-P3HT−MONA hybrids is shown in Figure S3a (Supporting Information). By showing a shorter PL lifetime, it directly shows that the charge separation at interface between P3HT and the oxide nanostructures is enhanced by the Fano resonance-induced electric field generated via the green-light irradiated Au@silica NPs in the hybrid.

Dynamics of charge recombination at the interfaces between oxide nanostructure and P3HT in the two cells, which are determined by IS with a transmission model,[14,22] are shown in Figure 6a. The IS measurements are conducted at V_{OC} of the hybrid solar cells under various intensities of green light (530 nm) irradiation. Figure 6a reveals that the electron lifetimes (τ_n) in the oxide nanostructures are functions of conductivity in the electron acceptors.[22] Moreover, the electron lifetimes in the P3HT-based NAFSC-1 are comparable to those in the P3HT−MONA solar cell. The Au-content-dependent electron lifetimes in the P3HT-based NAFSCs measured under a light intensity of 90 mW cm^{-2} are shown in Figure S3b (Supporting Information). The IS results indicate that the incorporation of the Au@silica NPs does not significantly influence the charge recombination inside the active layer. It is attributed to the electrically insulating surface of the silica shell, which efficiently prevents the rapid recombination of the photocarriers on the surface of bare Au NPs.

Charge transport properties of the P3HT−MONA solar cells with and without incorporating Au@silica NPs are further investigated by IMPS with a green light (530 nm) irradiation. The dynamics of electron transport in the metal oxide nanoarchitecture of the two solar cells are illustrated in Figure 6a. It shows that electron transit (transport) times (τ_t) in the P3HT-based NAFSC-1 are slightly longer than those in the P3HT−MONA cell. Moreover, the electron transit times in the hybrid solar cells increase with the amount of incorporated Au@silica NPs, as shown in Figure S3c (Supporting Information). The electron transport from ZnO NP/P3HT hybrid to the TiO_2 NR/FTO substrate may be retarded by the asymmetric quadrupole of Fano resonances generated via the green-light irradiated Au@silica NPs in the hybrid, as shown in Figure 1c, which is not parallel to the efficient electron transport direction.

The electron collection efficiencies (η_c) of the two hybrid solar cells are estimated from the electron transit time and lifetime with the relation of $\eta_c = 1 - (\tau_t/\tau_n)$.[23] As shown in Figure 6b, superior electron collection efficiencies are obtained in both P3HT−MONA solar cell and P3HT-based NAFSC-1. An electron collection efficiency of ∼97% is maintained in the P3HT-based NAFSC-1. Figure S3d (Supporting Information) demonstrates the Au-content-dependent electron collection efficiencies in the Au@silica NP-incorporated hybrid solar cells, which are estimated from Figure S3b,c (Supporting Information). The electron collection efficiency of the cell decreases as the amount of the incorporated Au@silica NPs increases.

Due to the high electron collection efficiency in the P3HT-based NAFSC-1 with a TiO_2−NR thickness of 650 nm, the photovoltaic performance of the P3HT-based NAFSC-1 is further optimized in terms of the thickness of the TiO_2 NR

array. The photovoltaic parameters of the P3HT-based NAFSCs with various TiO_2−NR thicknesses are shown in Figure 7a. With a TiO_2−NR thickness of 900 nm, an efficiency

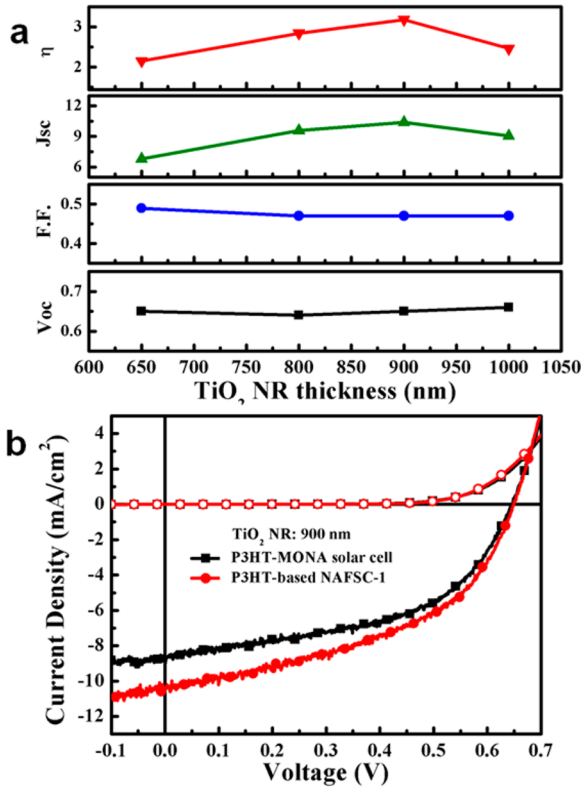

Figure 7. (a) Photovoltaic properties of P3HT-based NAFSCs-1 with various NR-array thicknesses. (b) *J*−*V* curves of P3HT−MONA solar cell and P3HT-based NAFSC-1 with a TiO_2−NR thickness of 900 nm.

of 3.18% with a J_{sc} of 10.38 mA cm^{-2}, a V_{OC} of 0.65 V, and a fill factor (FF) of 0.47 is achieved in the P3HT-based NAFSC. The *J*−*V* curves of the optimized P3HT-based NAFSC and the corresponding P3HT−MONA solar cell are shown in Figure 7b. With the addition of Au@silica NPs into the active layer, the J_{sc} improves by 17.8%, from 8.81 to 10.38 mA cm^{-2}, and the efficiency enhances by 10.4%, from 2.88 to 3.18%. (See Figure S4 and Table S3 in the Supporting Information for the statistical photovoltaic parameters of the two cells.) To the best of our knowledge, this is the highest efficiency ever reported for the metal oxide−P3HT hybrid solar cell without any interfacial modification.

The performance of the metal oxide−P3HT hybrid solar cells has been significantly improved with the assistance of Fano resonances via the incorporation of the Au@silica NPs into the active layer. As shown in Figure 3, a 30% enrichment of the J_{sc} can be attained in the P3HT-based NAFSC. However, Figures 2a and 5 respectively show that the absorbance of the active layer in the wavelength range of 400−600 nm and the exciton generation rate are not enhanced by the incorporation of Au@silica NPs. Moreover, Figure 4 reveals that the spectral range of EQE enhancement does not comply with the absorption spectrum of Au@silica NPs. These results suggest that the Fano resonance-induced light absorption and trapping on the photovoltaic performance of the Fano resonance solar cells is absent. As shown in Figure 1c, the asymmetric quadrupole of Fano resonance on the surface of the Au@silica NP, which is induced by the interaction between dielectric silica and surface plasmonic resonance of the Au NP core, possesses locally weaker energy densities compared to the region far from the NP in the overlayer. The FDTD simulation result confirms that the addition of the Au@silica NP in the ZnO NP/P3HT hybrid is not able to improve the light harvesting of the active layer by the LSPR effect due to the existence of the silica shell.

Nevertheless, the asymmetric quadrupole on the surface of the Au@silica NP shown in Figure 1c is a quasi-static Fano resonance, which produces a steady quasi-static electric field. The quasi-static electric field of the asymmetric quadrupolar Fano resonance penetrating into the active layer facilitates the charge separation. The FDTD simulation result explains the TRPL results in Figure 5b: the charge separation at the interface between P3HT and oxide nanostructures is enhanced by the Fano resonance-induced electric field triggered via the green-light irradiated Au@silica NPs in the hybrid. In contrast, the electric field in the high-energy density region of Figure 1c, which originates from the incident light, does not contribute to the enhancement of the charge separation in the active layer due to its high frequency of $10^{14,15}$ Hz. Therefore, the simulation result is consistent with the summary of EQE, PL, and TRPL investigations: the improvement of J_{sc} by the Fano resonance through the incorporation of Au@silica NPs into the P3HT−MONA solar cell originates from the enhancement of charge separation rather than the light absorption.

The Fano resonance effect on the cells is absent at the wavelengths out of the Au@silica NPs absorption range during the EQE measurements. We suggest that the enhancement of EQE values measured by the ordinary way (Figure 4a) is ascribed to the increase of the degree of P3HT order in the hybrid when incorporating the Au@silica NPs, as determined by Raman spectra (Figure 2b). Therefore, compared to that of the P3HT−MONA hybrid solar cell, a 30% enrichment of the J_{sc} in the P3HT-based NAFSC is mainly attributed to the Fano resonance-enhanced charge separation and the increase of the degree of P3HT order in the hybrid by the addition of the Au@silica NPs. Moreover, with the examinations of dynamics of charge separation, recombination, and transport in the hybrid solar cells, we conclude that the photovoltaic performance of the P3HT-based NAFSC is optimized with an appropriate content of Au@silica NPs due to the opposite trends in charge separation efficiency and electron collection efficiency influenced by the asymmetric quadrupolar electric field of Fano resonance.

With the same Au content in the hybrids of the P3HT-based NAFSCs, the extent of the improvements in the J_{sc} and efficiency of the cell shown in Figure 7b are inferior to those shown in Figure 3. Because the size of the Au@silica NP is comparable to the space between the TiO_2 NRs, as shown in Figure S5 (Supporting Information), the Au@silica NPs may be ineffectually incorporated into the ZnO NP/P3HT hybrid within the interstices of TiO_2 NRs. Namely, the Au@silica NPs may mainly exist in the overlayer portion of the P3HT-based NAFSC. When thickening the TiO_2 NR array, the bottom portion of the ZnO NP/P3HT hybrid within the interstices of TiO_2 NRs, which is not influenced by the asymmetric quadrupole of Fano resonances, may essentially contribute to the increases of the J_{sc} and efficiency of the hybrid cell. Therefore, compared to the cell with a shorter TiO_2 NR array, the extent of the performance improvement by Au@silica NP incorporation reduces the overall efficiency-optimized P3HT-based NAFSC.

4. CONCLUSIONS

A P3HT-based nanoarchitectural Fano solar cell is demonstrated in this work. The FDTD simulation shows the existence of an asymmetric quadrupole of Fano resonance on the surface of Au@silica NP as being incorporated into the P3HT−MONA hybrid. In the absence of the enhancement of the light absorption, a 30% enrichment of the J_{sc} is attained in the P3HT-based NAFSC compared to that of the corresponding P3HT−MONA solar cell. The increase in J_{sc} is mainly attributed to the Fano resonance-enhanced charge separation and the increase of the degree of P3HT order in the hybrid by the addition of the Au@silica NPs. The photoconversion efficiency of the P3HT-based NAFSC is optimized with an appropriate content of Au@silica NPs due to the opposite trends in charge separation efficiency and electron collection efficiency influenced by the asymmetric quadrupolar electric field of Fano resonance.

■ ASSOCIATED CONTENT

Ⓢ Supporting Information

Decomposition of simulated energy density distribution around Au@silica NP in ZnO NP/P3HT hybrid; PL decay times of Fano-P3HT−MONA hybrids with various Au@silica NP contents; electron lifetimes, electron transit times, and charge collection efficiencies in the P3HT-based NAFSCs with various Au@silica NP contents; SEM image of TiO_2 NR array. This material is available free of charge via the Internet at http://pubs.acs.org.

■ AUTHOR INFORMATION

Corresponding Author

*E-mail: wujj@mail.ncku.edu.tw.

Author Contributions

‖These authors contributed equally to this work.

Notes

The authors declare no competing financial interest.

■ ACKNOWLEDGMENTS

Financial support from the Headquarters of University Advancement at the National Cheng Kung University, which is sponsored by the Ministry of Education, Taiwan, and from the Ministry of Science and Technology in Taiwan under Contract No. 102-2221-E-006-215-MY3 is gratefully acknowledged.

■ REFERENCES

(1) Mayer, A. C.; Scully, S. R.; Hardin, B. E.; Rowell, M. W.; McGehee, M. D. Polymer-Based Solar Cells. *Mater. Today* **2007**, *10*, 28−33.

(2) Gunes, S.; Neugebauer, H.; Sariciftci, N. S. Conjugated Polymer-Based Organic Solar Cells. *Chem. Rev.* **2007**, *107*, 1324−1338.

(3) Lizin, S.; Van Passel, S.; De Schepper, E.; Maes, W.; Lutsen, L.; Manca, J.; Vanderzande, D. Life Cycle Analyses of Organic Photovoltaics: A Review. *Energy Environ. Sci.* **2013**, *6*, 3136−3149.

(4) Kumar, P.; Chand, S. Recent Progress and Future Aspects of Organic Solar Cells. *Prog. Photovoltaics* **2012**, *20*, 377−415.

(5) Chen, W.; Nikiforov, M. P.; Darling, S. B. Morphology Characterization in Organic and Hybrid Solar Cells. *Energy Environ. Sci.* **2012**, *5*, 8045−8074.

(6) Stratakis, E.; Kymakis, E. Nanoparticle-Based Plasmonic Organic Photovoltaic Devices. *Mater. Today* **2013**, *16*, 133−146.

(7) Gan, Q.; Bartoli, F. J.; Kafafi, Z. H. Plasmonic-Enhanced Organic Photovoltaics: Breaking the 10% Efficiency Barrier. *Adv. Mater.* **2013**, *25*, 2385−2396.

(8) Li, X.; Choy, W. C. H.; Lu, H.; Sha, W. E. I.; Ho, A. H. P. Efficiency Enhancement of Organic Solar Cells by Using Shape-Dependent Broadband Plasmonic Absorption in Metallic Nanoparticles. *Adv. Funct. Mater.* **2013**, *23*, 2728−2735.

(9) Lu, L.; Luo, Z.; Xu, T.; Yu, L. Cooperative Plasmonic Effect of Ag and Au Nanoparticles on Enhancing Performance of Polymer Solar Cells. *Nano Lett.* **2012**, *13*, 59−64.

(10) Wu, J.-L.; Chen, F.-C.; Hsiao, Y.-S.; Chien, F.-C.; Chen, P.; Kuo, C.-H.; Huang, M. H.; Hsu, C.-S. Surface Plasmonic Effects of Metallic Nanoparticles on the Performance of Polymer Bulk Heterojunction Solar Cells. *ACS Nano* **2011**, *5*, 959−967.

(11) Chen, B.; Zhang, W.; Zhou, X.; Huang, X.; Zhao, X.; Wang, H.; Liu, M.; Lu, Y.; Yang, S. Surface Plasmon Enhancement of Polymer Solar Cells by Penetrating Au/SiO_2 Core/Shell Nanoparticles into All Organic Layers. *Nano Energy* **2013**, *2*, 906−915.

(12) Janković, V.; Yang, Y.; You, J.; Dou, L.; Liu, Y.; Cheung, P.; Chang, J. P. Active Layer-Incorporated, Spectrally Tuned Au/SiO_2 Core/Shell Nanorod-Based Light Trapping for Organic Photovoltaics. *ACS Nano* **2013**, *7*, 3815−3822.

(13) Xu, X.; Kyaw, A. K. K.; Peng, B.; Zhao, D.; Wong, T. K. S.; Xiong, Q.; Sun, X. W.; Heeger, A. J. A Plasmonically Enhanced Polymer Solar Cell With Gold−Silica Core−Shell Nanorods. *Org. Electron.* **2013**, *14*, 2360−2368.

(14) Liao, W.-P.; Wu, J.-J. Efficient Electron Collection in Hybrid Polymer Solar Cells: In-Situ-Generated ZnO/Poly(3-hexylthiophene) Scaffolded by a TiO_2 Nanorod Array. *J. Phys. Chem. Lett.* **2013**, *4*, 1983−1988.

(15) Chen, H.; Shao, L.; Man, Y. C.; Zhao, C.; Wang, J.; Yang, B. Fano Resonance in (Gold Core)−(Dielectric Shell) Nanostructures without Symmetry Breaking. *Small* **2012**, *8*, 1503−1509.

(16) Yang, Z.-J.; Wang, Q.-Q.; Lin, H.-Q. Tunable Two Types of Fano Resonances in Metal−Dielectric Core−Shell Nanoparticle Clusters. *Appl. Phys. Lett.* **2013**, *103*, 111115.

(17) Hsu, S.-C.; Liao, W.-P.; Lin, W.-H.; Wu, J.-J. Modulation of Photocarrier Dynamics in Indoline Dye-Modified TiO_2 Nanorod Array/P3HT Hybrid Solar Cell with 4-*tert*-Butylpridine. *J. Phys. Chem. C* **2012**, *116*, 25721−25726.

(18) Liao, W.-P.; Hsu, S.-C.; Lin, W.-H.; Wu, J.-J. Hierarchical TiO_2 Nanostructured Array/P3HT Hybrid Solar Cells with Interfacial Modification. *J. Phys. Chem. C* **2012**, *116*, 15938−15945.

(19) Liao, W.-P.; Wu, J.-J. Wet Chemical Route to Hierarchical TiO_2 Nanodendrite/Nanoparticle Composite Anodes for Dye-Sensitized Solar Cells. *J. Mater. Chem.* **2011**, *21*, 9255−9262.

(20) Kobayashi, Y.; Inose, H.; Nakagawa, T.; Gonda, K.; Takeda, M.; Ohuchi, N.; Kasuya, A. Control of Shell Thickness in Silica-Coating of Au Nanoparticles and Their X-Ray Imaging Properties. *J. Colloid Interface Sci.* **2011**, *358*, 329−333.

(21) Kim, M. S.; Kang, M. G.; Guo, L. J.; Kim, J. Choice of Electrode Geometry for Accurate Measurement of Organic Photovoltaic Cell Performance. *Appl. Phys. Lett.* **2008**, *92*, 133301.

(22) Fabregat-Santiago, F.; Bisquert, J.; Cevey, L.; Chen, P.; Wang, M.; Zakeeruddin, S. M.; Grätzel, M. Electron Transport and Recombination in Solid-State Dye Solar Cell with Spiro-OMeTAD as Hole Conductor. *J. Am. Chem. Soc.* **2008**, *131*, 558−562.

(23) Wong, D. K.-P.; Ku, C.-H.; Chen, Y.-R.; Chen, G.-R.; Wu, J.-J. Enhancing Electron Collection Efficiency and Effective Diffusion Length in Dye-Sensitized Solar Cells. *ChemPhysChem* **2009**, *10*, 2698−2702.

(24) Yang, J.; You, J.; Chen, C.-C.; Hsu, W.-C.; Tan, H.-R.; Zhang, X. W.; Hong, Z.; Yang, Y. Plasmonic Polymer Tandem Solar Cell. *ACS Nano* **2011**, *5*, 6210−6217.

(25) Tsoi, W. C.; James, D. T.; Kim, J. S.; Nicholson, P. G.; Murphy, C. E.; Bradley, D. D. C.; Nelson, J.; Kim, J.-S. The Nature of In-Plane Skeleton Raman Modes of P3HT and Their Correlation to the Degree of Molecular Order in P3HT:PCBM Blend Thin Films. *J. Am. Chem. Soc.* **2011**, *133*, 9834−9843.

(26) Du, P.; Cao, Y.; Li, D.; Liu, Z.; Kong, X.; Sun, Z. Synthesis of Thermally Stable Ag@TiO_2 Core-Shell Nanoprisms and Plasmon-Enhanced Optical Properties for a P3HT Thin Film. *RSC Adv.* **2013**, *3*, 6016−6021.
(27) Tan, K.-S.; Chuang, M.-K.; Chen, F.-C.; Hsu, C.-S. Solution-Processed Nanocomposites Containing Molybdenum Oxide and Gold Nanoparticles as Anode Buffer Layers in Plasmonic-Enhanced Organic Photovoltaic Devices. *ACS Appl. Mater. Interfaces* **2013**, *5*, 12419−12424.